

## Magnetocaloric effect in kinetically frustrated diamond chains

M. S. S. Pereira, F. A. B. F. de Moura, and M. L. Lyra

*Instituto de Física, Universidade Federal de Alagoas, 57072-970 Maceió-AL, Brazil*

(Received 3 December 2008; published 20 February 2009)

We investigate the magnetocaloric effect in a diamond chain model on which competing interactions result from the local quantum hopping of interstitial  $S=1/2$  spins which are intercalated between nodal Ising spins. The model is exactly solvable by using exact diagonalization and the decoration-iteration mapping onto the one-dimensional Ising model with effective parameters depending on the temperature and the external magnetic field. We analyze the thermodynamic behavior of the effective parameters in light of the ground-state ordering and the level crossing of the low-lying excited states. Further, we investigate the magnetocaloric effect on this spin chain model by computing isoentropy curves in the temperature versus external field parameter space, as well as the adiabatic cooling rate. We show that the adiabatic cooling rate exhibits a pronounced valley-peak structure in the vicinity of the critical fields associated with zero-temperature phase transitions.

DOI: [10.1103/PhysRevB.79.054427](https://doi.org/10.1103/PhysRevB.79.054427)

PACS number(s): 75.30.Sg, 75.10.Pq, 75.50.Gg

### I. INTRODUCTION

The magnetocaloric effect consists on the heating or cooling of a thermally insulated magnetic substance by changing an external field. It has been used as a practical procedure to reach ultralow temperatures in a process known as adiabatic demagnetization. This process is also the basis for magnetic refrigeration, whose working substance is a magnetic sample instead of the gas used in the conventional refrigeration technology.<sup>1</sup> For low-temperature cooling applications, the standard refrigerant materials are paramagnetic salts. These systems basically contain noninteracting magnetic dipoles. A weak coupling of the magnetic dipoles with the lattice is the channel for the heat transfer process. In paramagnets, the temperature decreases linearly as the magnetic field is decreased during an adiabatic process. In order to improve the adiabatic cooling rate  $\partial T/\partial H|_S$  higher densities of magnetic dipoles are required. However, the residual interaction between the magnetic dipoles may induce spin ordering in this regime. The reduced entropy due to the spin-spin coupling thus limits the efficiency of the adiabatic demagnetization process.

Due to the recent advances in the experimental techniques of engineering and synthesis of new magnetic materials, there has been a growing interest in the development of new compounds with an improved magnetocaloric effect. A giant magnetocaloric effect was reported in gadolinium-based materials which is related to a first-order transition between two ferromagnetic phases.<sup>2</sup> New substances with an enhanced magnetocaloric effect have been recently discovered, which includes  $\text{La}(\text{Fe}, \text{Si})_{13}$ , MnAs-based,  $\text{Fe}_2\text{P}$ -based compounds, and Heusler alloys with their scientific aspects and industrial applicability are being widely investigated.<sup>3-6</sup> The underlying mechanism leading to an enhanced magnetocaloric effect in these materials is related to a large entropy excess that occurs at the vicinity of the first-order transitions exhibited by these compounds. Within this scenario, the presence of competing magnetic interactions plays a key role. The possibility of distinct ground states, which can be selected by varying an external magnetic field, allows for a fine tuning of the thermodynamic parameters leading to degenerate spin

ordering, and thus, to large adiabatic cooling rates. Enhanced magnetocaloric rates in frustrated spin models have been recently reported to demonstrate this mechanism.<sup>7-12</sup>

Low-dimensional magnetic systems with competing interactions are known to present a rich thermodynamic behavior.<sup>13-18</sup> One of the most intriguing features is the occurrence of magnetization plateaus. In this regime, the system does not respond to an external magnetic field. Magnetization plateaus were first predicted to occur in integer antiferromagnetic spin chains and later demonstrated to also emerge in chains with half-integer spins on trimerized and frustrated geometries. Among the several models of low-dimensional frustrated systems, the quantum Heisenberg spin chain in a diamond topology with competing interactions has been largely explored.<sup>19-25</sup> This model exhibits magnetization plateaus and double peak structures in the thermodynamic response functions which reflect the interplay between the competing ground states. These signatures have been experimentally observed in the diamond chain compound  $\text{Cu}_3(\text{CO}_3)_2(\text{OH})_2$  known as azurite.<sup>26,27</sup>

Recently, we introduced an exactly solvable model containing localized nodal Ising-type spins and exchanging interstitial electrons in an anisotropic diamond chain topology.<sup>28</sup> In this model, the kinetic term associated with the interstitial delocalized electrons produces antiferromagnetic correlations leading to frustrated interactions. We showed that this model presents most of the features of frustrated low-dimensional spin chains such as magnetization plateaus and two peaks in the specific heat and magnetic susceptibility. Further, the model exhibits four distinct ground states which can be tuned by changing an external magnetic field or the transfer integral which governs the amplitude of the kinetic term. Actually, a more realistic model for the low-energy properties of magnetic materials with a diamond chain geometry should consider a Heisenberg Hamiltonian and electron hopping between distinct unit cells. However, the thermodynamic behavior of such extended model can only be obtained by approximate analytical solutions or, alternatively, by numerical studies of finite chains using exact diagonalization or density-matrix renormalization-group techniques. On the other hand, the restriction of internodal hopping and Ising nodal spins allows for an exact analytical

solution of the above Hamiltonian model while keeping the main ingredients, such as geometry, quantum fluctuations, frustration, and anisotropy, which are responsible for some of the most remarkable thermodynamic characteristics of frustrated diamond chain compounds.<sup>28</sup>

The existence of four possible ground states in the diamond chain model with mixed localized Ising and delocalized interstitial spins suggests that this model system has the essential ingredients needed to exhibit an enhanced magnetocaloric effect. Here, we will use the exact solution of this model, based on its exact mapping in the Ising spin chain with effective parameters, to compute the isoentropy curves, as well as the adiabatic cooling rate  $\partial T/\partial H|_S$ , as a function of the temperature and external field. We will show that enhanced magnetocaloric rates take place in the vicinity of the critical fields separating the possible ground states. We will analyze the most prominent features of the adiabatic cooling rate in light of the thermodynamic behavior of the effective exchange coupling and magnetic field. This paper is organized as follows. In Sec. II we will describe the model Hamiltonian and the exact solution of the associated partition function by means of the decoration-iteration transformation in the Ising spin chain. In Sec. III, we report the thermodynamic behavior of the effective exchange coupling and effective field for a typical value of the transfer integral for which all four possible ground states can be realized. In Sec. IV, we compute the magnetic entropy, reporting the curves of isoentropy to illustrate the adiabatic magnetocaloric effect, as well as the adiabatic cooling rate. The latter will be shown to reach low-temperature values that can be 1 order of magnitude larger than in paramagnets, specially in the vicinity of the critical fields. Finally, in Sec. V, we summarize our main results.

## II. KINETICALLY FRUSTRATED DIAMOND CHAIN MODEL

The diamond chain model, also known as  $AB_2$  chain, consists of linked unitary cells with two species of sites. Those sites of specie  $A$  form the chain nodes, while the sites of specie  $B$  are intercalated between the nodes. When localized spins are assumed to occupy each site of this chain and exchange couplings are allowed only between sites of different species, the ground state is unique irrespective of the relative magnitude and the nature of the exchange couplings  $J_1$  and  $J_2$  along each direction of the diamond cell. Frustration effects can only take place when antiferromagnetic couplings are allowed between sites of the same specie. Recently, we demonstrated that frustration can be kinematically produced by allowing the internodal spins to hop between the pairs of  $B$  sites of each unitary cell.<sup>28</sup>

For simplicity, we are going to consider both nodal and internodal spins as Ising variables  $\sigma$  and  $S$ , respectively. Further, we will restrict our analysis to the case of antiferromagnetic exchange couplings which produce a more diverse scenario regarding the ground state and thermodynamic behavior. A diagrammatic representation of the chain is shown in Fig. 1. The cell Hamiltonian  $\mathcal{H}_i$  can be written in a matrix form in the space state corresponding to the six pos-

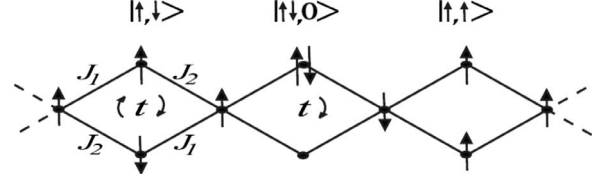


FIG. 1. Diagrammatic representation of the kinetically frustrated diamond chain model. Internodal spins with antiparallel spins are allowed to hop within the inner sites of each diamond unit with hopping probability amplitude  $t$ . The magnetic interactions are anisotropic with distinct exchange couplings along each direction of the unit cell. The state vectors illustrate the notation used in text.

sible configurations for the internodal spins. The two states with parallel internodal spins are eigenstates of the cell Hamiltonian. In these states, there is one spin in each site and the hopping is forbidden by the Pauli exclusion rule. These states are represented by the ket states  $|\uparrow, \uparrow\rangle$  and  $|\downarrow, \downarrow\rangle$ . In the absence of an external magnetic field, the corresponding eigenvalues can be written as  $\langle \uparrow, \uparrow | \mathcal{H}_i | \uparrow, \uparrow \rangle = -\langle \downarrow, \downarrow | \mathcal{H}_i | \downarrow, \downarrow \rangle = -(J_1 + J_2)(\sigma_i + \sigma_{i+1})$ , where  $\sigma_i$  and  $\sigma_{i+1}$  are the left and right nodal spins, respectively. The other four states with antiparallel internodal spins are mixed due to the single-particle hopping mechanism. Representing these states by the kets  $|\uparrow \downarrow, 0\rangle$ ,  $|\uparrow, \downarrow\rangle$ ,  $|0, \uparrow \downarrow\rangle$ , and  $|\downarrow, \uparrow\rangle$ , the cell Hamiltonian in this subspace can be written as

$$\mathcal{H}_i = \begin{pmatrix} 0 & t & 0 & t \\ t & -\Delta J(\sigma_i - \sigma_{i+1}) & t & 0 \\ 0 & t & 0 & t \\ t & 0 & t & \Delta J(\sigma_i - \sigma_{i+1}) \end{pmatrix},$$

where  $t$  is the hopping amplitude between internodal sites and  $\Delta J = J_1 - J_2$  is the exchange mismatch accounting for the anisotropy of the magnetic interactions within the diamond cell. Notice that the ket states with antiparallel internodal spins are not stationary. The Hamiltonian eigenstates will be composed by the linear superpositions of states that diagonalize the cell Hamiltonian. In the regime of large hopping amplitudes, the low-energy eigenstate becomes one of these linear superpositions of antiparallel internodal spins states. This feature leads to an antiferromagnetic correlation between the internodal spins that can effectively produce frustration effects. In the presence of a magnetic external field, a diagonal term has to be added to the cell Hamiltonian, which takes the form

$$\mathcal{H}_i(H) = \mathcal{H}_i(H=0) - \frac{H}{2}(\sigma_i + \sigma_{i+1}) - H(S_{i,1} + S_{i,2}), \quad (1)$$

where  $S_{i,j}$  ( $j=1,2$ ) identifies each of the internodal spins at cell  $i$ . The external field favors the parallel alignment of the spins, which competes with the kinetically induced antiferromagnetic coupling between the internodal spins.

By employing an exact diagonalization of the cell Hamiltonian, the above diamond chain model was shown to exhibit four possible ground states, depending on the relation among the hopping amplitude  $t$ , the external field  $H$ , and the exchange mismatch  $\Delta J$ .<sup>28</sup> A saturated paramagnetic (SPA) state

with all spins aligned in the field direction is the ground state at high magnetic fields. The system can also assume a ferrimagnetic (FRI) ground state, on which the internodal spins are aligned parallel to the external field while the nodal spins are aligned antiparallel to the field. In these two states, the hopping mechanism is suppressed because the internodal spins are parallel to each other. The other possible ground states are the unsaturated paramagnetic (UPA), with nodal spins parallel to the field, and the nodal antiferromagnetic (NAF) state, with nodal spins pointing in opposite directions. In the later two states, the internodal spins become antiferromagnetically correlated. In the parameter space composed of the magnetic field and exchange mismatch, all these phases can be reached when the hopping amplitude is in the range  $1 < t/|J_1| < 2$ , where  $J_1$  is assumed as the stronger exchange coupling.

The thermodynamic properties of the above diamond chain model can be obtained after the partial trace over the degrees of freedom associated with the possible configurations of the internodal spins. This procedure allows us to map the thermodynamics of the original model on that of an Ising chain with effective exchange coupling and external field. Such mapping, known as a decoration-iteration transformation,<sup>29</sup> has been extensively used to investigate the thermodynamic behavior of several decorated Ising systems. This technique usually provides the exact solution for the thermodynamic behavior, thus allowing for a deeper understanding of several magnetic phenomena.<sup>30–37</sup> For the present model, the mapping consists in defining the effective parameters through the identity

$$\sum_k e^{-\beta \lambda_k(\sigma_i, \sigma_{i+1})} = \gamma e^{\beta J_{\text{eff}} \sigma_i \sigma_{i+1} + (1/2)\beta H_{\text{eff}}(\sigma_i + \sigma_{i+1})}, \quad (2)$$

where  $\lambda_k(\sigma_i, \sigma_{i+1})$  are the eigenvalues of the cell Hamiltonian for a given configuration of the nodal spins and  $\beta = 1/k_B T$ . The partition function of the diamond chain model can be written as  $Z(T, J_1, J_2, t, H) = \gamma^N Z_{\text{Ising}}(T, J_{\text{eff}}, H_{\text{eff}})$ , with

$$Z_{\text{Ising}}(T, J_{\text{eff}}, H_{\text{eff}}) = \{e^{k_{\text{eff}}} \cosh h_{\text{eff}} + [e^{2k_{\text{eff}}} \cosh^2 h_{\text{eff}} - 2 \sinh(2k_{\text{eff}})]^{1/2}\}^N, \quad (3)$$

where  $k_{\text{eff}} = \beta J_{\text{eff}}$ ,  $h_{\text{eff}} = \beta H_{\text{eff}}$ ,  $N$  is the number of diamond cells, and periodic boundary conditions were assumed. By considering all possible configurations of the nodal spins of a unitary diamond cell, the set of equations resulting from Eq. (2) can be solved to obtain the parameters  $\gamma$ ,  $J_{\text{eff}}$ , and  $H_{\text{eff}}$ . After a straightforward algebra, one can write the effective field and exchange coupling in the following forms:

$$H_{\text{eff}} = H + \frac{1}{2\beta} \ln A - \frac{1}{2\beta} \ln B, \quad (4)$$

$$J_{\text{eff}} = \frac{1}{4\beta} \ln A + \frac{1}{4\beta} \ln B - \frac{1}{2\beta} \ln C, \quad (5)$$

where

$$A = e^{-\beta(4|J_1|-2|\Delta J|-2H)} + e^{-\beta(-4|J_1|+2|\Delta J|+2H)} + 2 + 2 \cosh(2\beta t), \quad (6)$$

$$B = e^{-\beta(-4|J_1|+2|\Delta J|-2H)} + e^{-\beta(4|J_1|-2|\Delta J|+2H)} + 2 + 2 \cosh(2\beta t), \quad (7)$$

$$C = 2 + 2 \cosh(2\beta H) + 2 \cosh[2\beta \sqrt{(\Delta J)^2 + t^2}]. \quad (8)$$

### III. THERMODYNAMIC BEHAVIOR OF THE EFFECTIVE PARAMETERS

The thermodynamic behavior of the effective parameters as a function of the applied magnetic field and temperature can be analyzed in more detail by considering separately the cases for which the ground state at  $H=0$  is FRI and NAF. We will consider the hopping amplitude in the range  $1 < t/|J_1| < 2$ , for which the zero-field ground state can be controlled by varying the exchange mismatch  $\Delta J$ . The typical behavior starting from a FRI zero-field ground state is depicted in Fig. 2, where we show the field dependence of the effective parameters at several temperatures. Four distinct regimes can be identified, specially at low temperatures. Notice that the effective field is negative at low temperatures and external fields, which reflects the fact that the predominant ordering of the nodal spins in the FRI state is antiparallel to the external field direction.

The thermodynamic behavior of the effective parameters for the case of a NAF ground state at zero field is shown in Fig. 3. Here, we also have four distinct regimes. The effective field is positive in all regimes. However, the effective coupling becomes negative at low fields due to the antiferromagnetic ordering of the nodal spins in the NAF state. At intermediate fields, the effective coupling becomes ferromagnetic, thus leading to the UPA ordering. For this ground state, the effective field exhibits a plateau. At higher fields, the SPA state is the most stable one and the chain becomes effectively decoupled. The bounds of the four regimes for the effective parameters at  $T=0$  and their corresponding expressions are summarized in Table I. These bounds identify the regions of physical parameters with distinct sets of Hamiltonian eigenstates corresponding to the minimal cell energy for each one of the three relevant configurations of the nodal spins.

Based on the above analysis of the effective parameters, we can provide a phase diagram, revealing a more detailed structure than the one presented in Ref. 28. Besides the bounds between the different ground states, we can also delimit the regimes for the field dependence of the effective coupling. The complete phase diagram for the particular case of  $t/|J_1|=1.5$  is shown in Fig. 4. For a given value of the exchange mismatch, the effective coupling is field independent at low fields. Then, it starts to grow until reaching a maximum value. After that, it decreases until vanishing at a specific field value, above which the chain becomes effectively decoupled. It is important to mention that the bounds between the distinct ground states take place when level crossings involve the lower-energy state. However, the

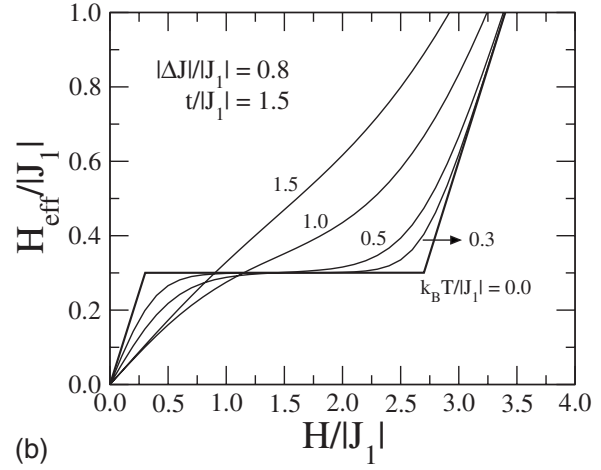
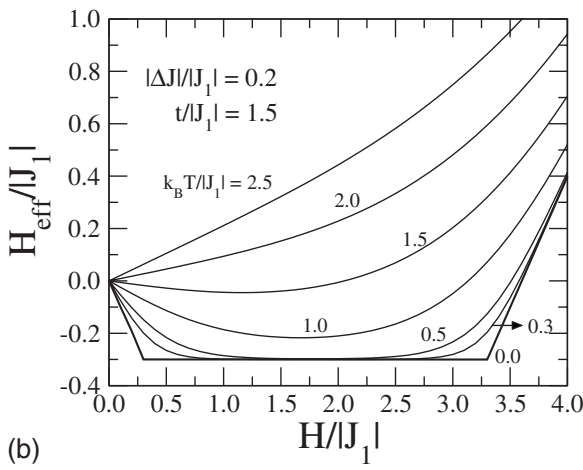
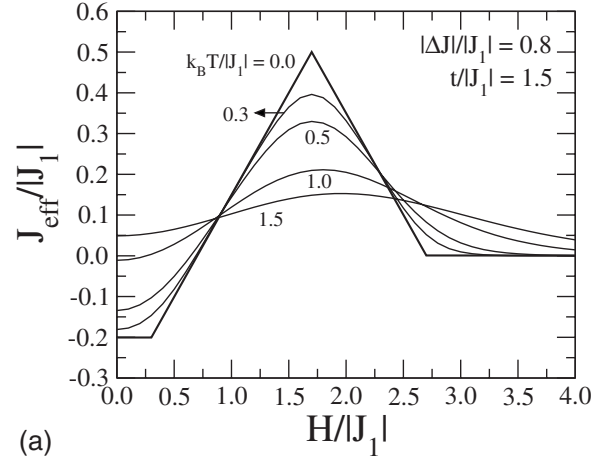
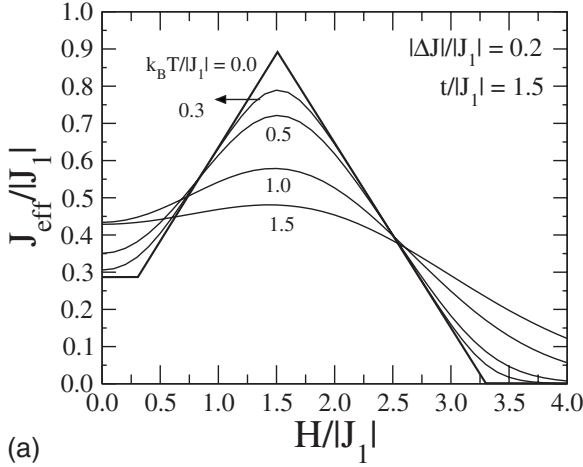


FIG. 2. Field dependence of the (a) effective exchange coupling and (b) effective magnetic field for different temperatures. Here, we used  $t/|J_1|=1.5$  and  $|\Delta J|/|J_1|=0.2$  for which the zero-field ground state is FRI. Four distinct regimes for the effective parameters are clearly seen at low temperatures. The negative values of the effective field reflect the fact that the nodal spins align contrary to the external field in the FRI ground state. The chain becomes effectively decoupled at high magnetic fields.

bounds between the distinct regimes of the effective parameters are determined by level crossings between excited states.

IV. ADIABATIC MAGNETOCALORIC EFFECT

The existence of several possible ground states that can be tuned by an external field makes the present model a good candidate to exhibit an enhanced magnetocaloric effect. This feature is mainly related to the expected increase in the magnetic entropy at the vicinity of the transition between these states. Although the present one-dimensional model has only zero-temperature transitions, well-defined crossovers can still be fairly identified at finite temperatures.

The magnetic cooling is usually performed through a process of adiabatic demagnetization. During this process, the external magnetic field is adiabatically decreased, thus keeping the magnetic entropy constant. In Fig. 5, we show isoen-

FIG. 3. Field dependence of the (a) effective exchange coupling and (b) effective magnetic field for different temperatures. Here, we used  $t/|J_1|=1.5$  and  $|\Delta J|/|J_1|=0.8$  for which the zero-field ground state is NAF. Four distinct regimes for the effective parameters are still clearly seen at low temperatures. The negative values of the effective exchange coupling reflect the antiferromagnetic correlation between the nodal spins in the NAF ground state. The chain becomes effectively decoupled in the SPA ground state. The plateau in the effective field is associated with the fact that the competing UPA and FRI states have the same magnetic moment per unit cell.

trophy curves in the  $T \times H$  parameter space for two representative cases. In Fig. 5(a), we have chosen an exchange mismatch for which the zero-field ground state is FRI. According to the phase diagram, there is a single critical field in this case, corresponding to the transition between the FRI and the SPA states. This critical field can be clearly identified in the isoentropy diagram. In Fig. 5(b), the zero-field ground state is NAF. For this case, two critical fields are present, delimiting the transitions between the NAF and UPA states as well as between the UPA and SPA states. The largest adiabatic variation in the temperature is indeed observed at the vicinity of the critical fields. Large adiabatic cooling rates are achieved when the magnetic field approaches the critical points from above, while maximum heating rates take place when the field is further reduced below the critical points. This is the scenario that favors the use of frustrated magnetic materials as active substances to perform refrigerator cycles.

TABLE I. Distinct regimes for the effective exchange coupling and field at  $T=0$  and their corresponding expressions within each regime. For low magnetic fields  $H \leq |2|J_1| - |\Delta J| - t|$ , the expressions for the effective parameters depend on the sign of  $\delta = 2|J_1| - |\Delta J| - t$ .

External field regime	Effective coupling	Effective field
$H \leq  \delta $	$(\delta \geq 0) J_{\text{eff}} = 2 J_1  -  \Delta J  - \sqrt{(\Delta J)^2 + t^2}$ $(\delta \leq 0) J_{\text{eff}} = t - \sqrt{(\Delta J)^2 + t^2}$	$(\delta \geq 0) H_{\text{eff}} = -H$ $(\delta \leq 0) H_{\text{eff}} = +H$
$ \delta  \leq H \leq \sqrt{(\Delta J)^2 + t^2}$	$J_{\text{eff}} =  J_1  + \frac{t}{2} - \frac{ \Delta J }{2} - \sqrt{(\Delta J)^2 + t^2} + \frac{H}{2}$	$H_{\text{eff}} = t - 2 J_1  +  \Delta J $
$\sqrt{(\Delta J)^2 + t^2} \leq H \leq 2 J_1  -  \Delta J  + t$	$J_{\text{eff}} =  J_1  + \frac{t}{2} - \frac{ \Delta J }{2} - \frac{H}{2}$	$H_{\text{eff}} = t - 2 J_1  +  \Delta J $
$H \geq 2 J_1  -  \Delta J  + t$	$J_{\text{eff}} = 0$	$H_{\text{eff}} = -4 J_1  + 2 \Delta J  + H$

Following a particular isoentropy line, we can find two typical behaviors as the field intensity is decreased from values above the upper critical field. If the initial temperature and field values correspond to a thermodynamic state with entropy well above the residual entropy at the upper critical field  $S_{\text{res}} = k_B \ln 2$ , corresponding to the degenerate FRI and SPA [Fig. 5(a)] or UPA and SPA [Fig. 5(b)] states, the temperature has an overall decrease when the external magnetic field is decreased. However, the temperature reduction that can be attained is limited in this case and the isoentropy lines develop a plateau at low fields. On the other hand, when the initial state has an entropy smaller than  $k_B \ln 2$ , the tempera-

ture can be reduced without a minimal bound. In this case, the temperature decrease is monotonous if the initial field is above the upper critical field. The temperature dependence on the external field becomes nonmonotonous when the initial field is below its upper critical value. In the case where the zero-field ground state is NAF [Fig. 5(b)], a second isoentropy line with  $S_{\text{res}} = k_B \ln(1 + \sqrt{5})/2$ , corresponding to the degenerate NAF and UPA states,<sup>28,38,39</sup> delimits the range of entropy values for which zero temperature can be reached by adiabatic cooling. For entropies smaller than  $k_B \ln(1 + \sqrt{5})/2$ , zero-temperature adiabatic cooling can be reached as one approaches the field values corresponding to both NAF/UPA and UPA/SPA transitions. In the range  $k_B \ln(1 + \sqrt{5})/2 < S < k_B \ln 2$  zero-temperature cooling is only reachable approaching the UPA/SPA transition. For  $S > k_B \ln 2$ , zero temperature cannot be reached by adiabatic cooling. The maximum rate of adiabatic cooling at low temperatures is achieved either along the isoentropy line  $S = k_B \ln 2$  at the upper critical field or at  $S = k_B \ln(1 + \sqrt{5})/2$  at the lower critical field.

The adiabatic magnetocaloric rate  $\partial T / \partial H|_S$  gives a more quantitative description of the enhanced efficiency of the cooling process in the vicinity of the critical fields. In Fig. 6, we report the field dependence of the magnetocaloric rate for different temperatures for the case of a FRI zero-field ground state. The structure of valley peak near the critical field clearly signals the enhanced magnetocaloric effect at low temperatures. Such structure is smoothed by thermal fluctuations but can still be identified up to temperatures of the order of  $k_B T / |J_1| = 1$ . For much larger temperatures, the magnetocaloric rate displays only a slow dependence on  $H$ . Therefore, no significant effect due to the underlying frustrated interactions persists. The magnetocaloric rate for the case of a NAF zero-field ground state is shown in Fig. 7. Here, there are two peak-valley structures that can be identified at very low temperatures. The one at low magnetic fields corresponds to the transition between the NAF and the UPA states. The enhancing of the magnetocaloric effect close to this transition is quite sensitive to thermal fluctuations, becoming strongly suppressed even at intermediate temperatures. On the other hand, the signal associated with the UPA

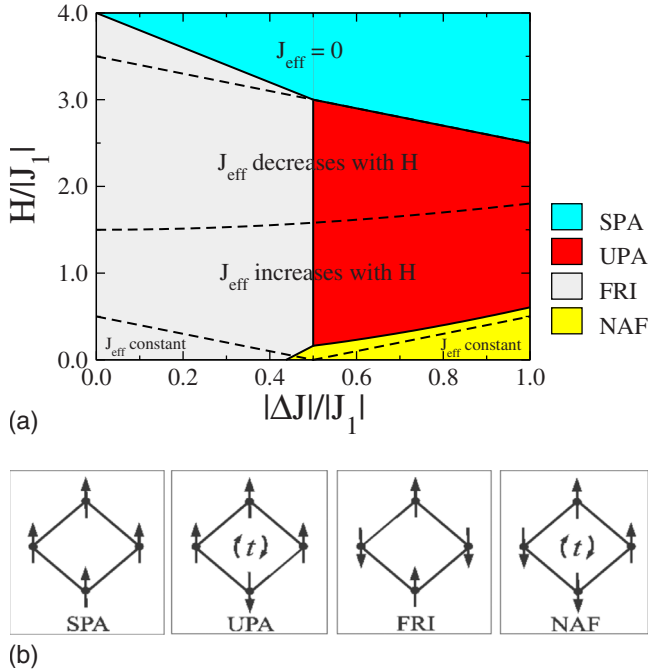


FIG. 4. (Color online) Ground-state phase diagram for  $t/|J_1| = 1.5$ . The dashed line delimits the different regimes for the field dependence of the effective exchange coupling. The analytic expressions for these lines are reported in Table I. The solid lines are the bounds between distinct ground states.

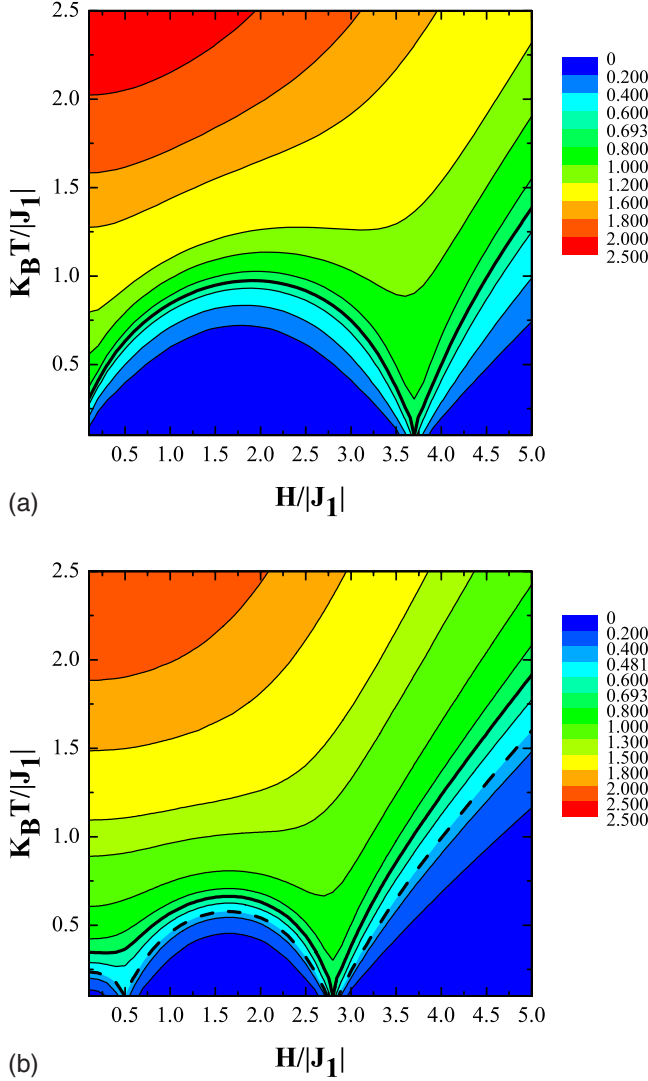


FIG. 5. (Color online) Curves of isoentropy in the  $T \times H$  parameter space for the particular case of hopping amplitude  $t/|J_1|=1.5$ . (a) Exchange mismatch  $|\Delta J|/|J_1|=0.2$  for which the zero-field ground state is FRI. A single critical field is present. (b) Exchange mismatch  $|\Delta J|/|J_1|=0.8$  for which the zero-field ground state is NAF. This case presents two critical fields. The isoentropy lines  $S = k_B \ln 2$  (thick solid) and  $k_B \ln(1 + \sqrt{5})/2 < S < k_B \ln 2$  (thick dashed) delimit distinct regimes for adiabatic cooling (see text). Maximum adiabatic cooling rates (slope of the isoentropy curves) take place near the critical fields at these special entropy values.

to SPA transition is more robust against thermal fluctuations. In comparison with the adiabatic magnetocaloric cooling rate of paramagnetic salts, which is simply given by  $\partial T / \partial H|_S = T/H$ , the maximum cooling rate at the vicinity of the critical field is about 1 order of magnitude larger at low temperatures.

V. SUMMARY AND CONCLUSIONS

In summary, we showed that the recently introduced model of a kinetically frustrated diamond chain can exhibit an enhanced adiabatic magnetocaloric rate. The model con-

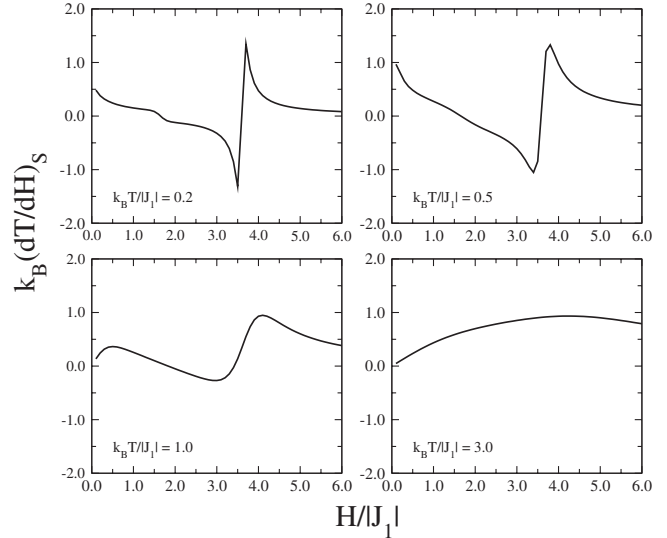


FIG. 6. Adiabatic magnetocaloric rate  $\partial T / \partial H|_S$  as a function of the external field for representative values of the temperature. For these plots, we used  $t/|J_1|=1.5$  and  $|\Delta J|/|J_1|=0.2$  for which the zero-field ground state is FRI. The valley-peak structure signals the enhanced magnetocaloric effect close to the FRI to SPA transition. The signal is suppressed by thermal fluctuations.

sists of an  $AB_2$  chain with anisotropic antiferromagnetic couplings between sites of different species. Further, a kinetic term allows the hopping of the internodal spins between the inner sites of each unit cell. Such hopping mechanism, associated with the Pauli exclusion principle, builds up antiferromagnetic correlations between the spins of the internodal sites which compete with the parallel correlation induced by

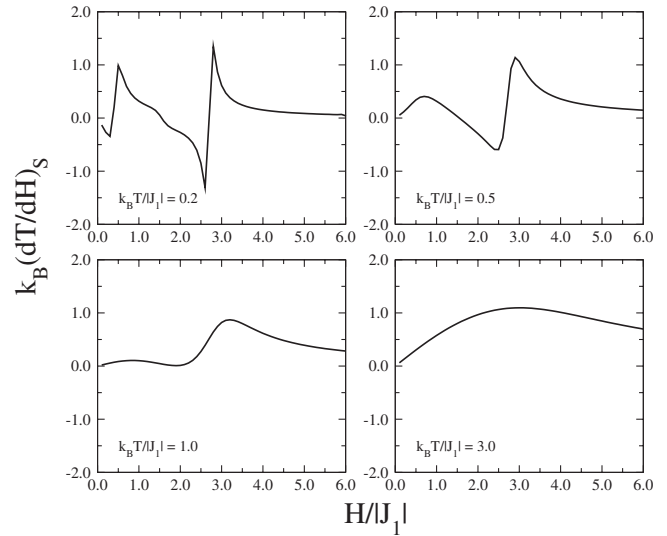


FIG. 7. Adiabatic magnetocaloric rate  $\partial T / \partial H|_S$  as a function of the external field for representative values of the temperature. For these plots we used  $t/|J_1|=1.5$  and  $|\Delta J|/|J_1|=0.8$  for which the zero-field ground state is NAF. The valley-peak structures signal the enhanced magnetocaloric effect close to the NAF to UPA and UPA to SPA transitions. The signal corresponding to the NAF to UPA transition is more sensitive to thermal fluctuations than the signal from the UPA to SPA transition.

the coupling with the nodal spins. The model has four possible ground states (SPA, UPA, FRI, and NAF) which can be tuned by varying the exchange mismatch, the hopping amplitude, and the applied magnetic field. The thermodynamic of this model has an exact solution through a decoration-iteration transformation that maps its partition function on that of an Ising chain with effective exchange coupling and magnetic field. We analyzed the thermodynamic behavior of the effective parameters. We showed that four regimes can be identified which differ from each other by the field dependence of the effective coupling at the ground state. We provided analytic expressions for the bounds of these regimes which complete the characterization of the ground-state phase diagram.

The possibility of tuning the ground-state configuration using the external magnetic field means that the ground state becomes degenerated at some critical fields. This scenario has been pointed in the literature as favorable for achieving an enhanced magnetocaloric effect. We explored such effect on the present model by computing the isoentropy curves of adiabatic demagnetization as well as the adiabatic magnetocaloric cooling rate. Our results showed clearly an enhanced

magnetocaloric effect. By choosing the initial thermodynamic state of the system to have an entropy smaller than the residual entropy at the critical fields for which the ground state is degenerated, we obtained that the temperature can be strongly reduced during a process of adiabatic demagnetization. Further, we showed that the magnetocaloric rate presents well-defined structures of valley peak at the vicinity of the critical fields, a welcome feature for the development of refrigerator cycles using magnetic materials as the active substance. Although the effect in the vicinity of the NAF to UPA transition is strongly suppressed by thermal fluctuations, the corresponding structure due to the UPA to SPA transition is quite robust with the valley-peak signal being well defined even at intermediate temperatures.

### ACKNOWLEDGMENTS

We are grateful for partial financial support from CAPES, CNPq, CNPq-Rede Nanobioestruturas, and FINEP (Brazilian research agencies) as well as from FAPEAL (Alagoas State research agency).

- 
- <sup>1</sup>A. M. Tishin and I. Spichkin, *The Magnetocaloric Effect and Its Applications* (Institute of Physics, Bristol, 2003).
- <sup>2</sup>V. K. Pecharsky and K. A. Gschneidner, Jr., *Phys. Rev. Lett.* **78**, 4494 (1997).
- <sup>3</sup>K. A. Gschneidner, Jr. and V. K. Pecharsky, *Annu. Rev. Mater. Sci.* **30**, 387 (2000).
- <sup>4</sup>K. A. Gschneidner, Jr., V. K. Pecharsky, and A. O. Tsokol, *Rep. Prog. Phys.* **68**, 1479 (2005).
- <sup>5</sup>K. A. Gschneidner, Jr. and V. K. Pecharsky, *J. Rare Earths* **24**, 641 (2006).
- <sup>6</sup>E. Brück, O. Tegus, D. T. C. Thanh, and K. H. J. Buschow, *J. Magn. Magn. Mater.* **310**, 2793 (2007).
- <sup>7</sup>J. Richter, *Low Temp. Phys.* **31**, 695 (2005).
- <sup>8</sup>M. E. Zhitomirsky and A. Honecker, *J. Stat. Mech.: Theory Exp.* (2004) P07012.
- <sup>9</sup>M. E. Zhitomirsky, *Phys. Rev. B* **67**, 104421 (2003).
- <sup>10</sup>J. Schnack, R. Schmidt, and J. Richter, *Phys. Rev. B* **76**, 054413 (2007).
- <sup>11</sup>H. Tsujii, C. R. Rotundu, T. Ono, H. Tanaka, B. Andraka, K. Ingersent, and Y. Takano, *Phys. Rev. B* **76**, 060406(R) (2007).
- <sup>12</sup>B. Schmidt, P. Thalmeier, and Nic Shannon, *Phys. Rev. B* **76**, 125113 (2007).
- <sup>13</sup>K. Totsuka, *Phys. Rev. B* **57**, 3454 (1998).
- <sup>14</sup>D. C. Cabra, A. Honecker, and P. Pujol, *Phys. Rev. Lett.* **79**, 5126 (1997).
- <sup>15</sup>A. Honecker, F. Mila, and M. Troyer, *Eur. Phys. J. B* **15**, 227 (2000).
- <sup>16</sup>A. Koga, K. Okunishi, and N. Kawakami, *Phys. Rev. B* **62**, 5558 (2000).
- <sup>17</sup>J. Schulenburg and J. Richter, *Phys. Rev. B* **65**, 054420 (2002).
- <sup>18</sup>Y.-C. Li and S.-S. Li, *Phys. Rev. B* **78**, 184412 (2008).
- <sup>19</sup>K. Okamoto, T. Tonegawa, Y. Takahashi, and M. Kaburagi, *J. Phys.: Condens. Matter* **11**, 10485 (1999).
- <sup>20</sup>T. Sakai and K. Okamoto, *Phys. Rev. B* **65**, 214403 (2002).
- <sup>21</sup>S. K. Pati, *Phys. Rev. B* **67**, 184411 (2003).
- <sup>22</sup>M. H. Oliveira, M. D. Coutinho-Filho, and E. P. Raposo, *Phys. Rev. B* **72**, 214420 (2005).
- <sup>23</sup>Y. C. Li, *J. Appl. Phys.* **102**, 113907 (2007).
- <sup>24</sup>H. J. Mikeska and C. Luckmann, *Phys. Rev. B* **77**, 054405 (2008).
- <sup>25</sup>R. R. Montenegro-Filho and M. D. Coutinho-Filho, *Phys. Rev. B* **78**, 014418 (2008).
- <sup>26</sup>H. Kikuchi, Y. Fujii, M. Chiba, S. Mitsudo, T. Idehara, T. Tonegawa, K. Okamoto, T. Sakai, T. Kuwai, and H. Ohta, *Phys. Rev. Lett.* **94**, 227201 (2005).
- <sup>27</sup>K. C. Rule, A. U. B. Wolter, S. Sullow, D. A. Tennant, A. Bruhl, S. Kohler, B. Wolf, M. Lang, and J. Schreuer, *Phys. Rev. Lett.* **100**, 117202 (2008).
- <sup>28</sup>M. S. S. Pereira, F. A. B. F. de Moura, and M. L. Lyra, *Phys. Rev. B* **77**, 024402 (2008).
- <sup>29</sup>I. Syozi, in *Phase Transitions and Critical Phenomena*, edited by C. Domb and M. S. Green (Academic, New York, 1972), Vol. 1.
- <sup>30</sup>M. L. Lyra and S. Coutinho, *Physica A* **155**, 232 (1989).
- <sup>31</sup>N. C. Eddeqaqi, M. Saber, A. El-Atri, and M. Kerouad, *J. Phys.: Condens. Matter* **11**, 5603 (1999).
- <sup>32</sup>J. Strečka and M. Jaščur, *Phys. Rev. B* **66**, 174415 (2002).
- <sup>33</sup>V. R. Ohanyan and N. S. Ananikian, *Phys. Lett. A* **307**, 76 (2003).
- <sup>34</sup>J. Oitmaa and W. H. Zheng, *Physica A* **328**, 185 (2003).
- <sup>35</sup>L. Čanová, J. Strečka, and M. Jaščur, *J. Phys.: Condens. Matter* **18**, 4967 (2006).
- <sup>36</sup>S. Mat'ášovská and M. Jaščur, *Physica A* **383**, 339 (2007).
- <sup>37</sup>J. Strečka, L. Čanová, and M. Jaščur, *Phys. Rev. B* **76**, 014413 (2007).
- <sup>38</sup>C. Domb, *Adv. Phys.* **9**, 149 (1960).
- <sup>39</sup>A. A. Ovchinnikov, D. V. Dmitriev, V. Y. Krivnov, and V. O. Cheranovskii, *Phys. Rev. B* **68**, 214406 (2003).